

DESY-13-234

September 10, 2018

Photoproduction of isolated photons, inclusively and with a jet, at HERA

ZEUS Collaboration

Abstract

The photoproduction of isolated photons, both inclusive and together with a jet, has been measured with the ZEUS detector at HERA using an integrated luminosity of 374 pb^{-1} . Differential cross sections are presented in the isolated-photon transverse-energy and pseudorapidity ranges $6 < E_T^\gamma < 15 \text{ GeV}$ and $-0.7 < \eta^\gamma < 0.9$, and for jet transverse-energy and pseudorapidity ranges $4 < E_T^{\text{jet}} < 35 \text{ GeV}$ and $-1.5 < \eta^{\text{jet}} < 1.8$, for exchanged-photon virtualities $Q^2 < 1 \text{ GeV}^2$. Differential cross sections are also presented for inclusive isolated-photon production as functions of the transverse energy and pseudorapidity of the photon. Higher-order theoretical calculations are compared to the results.

The ZEUS Collaboration

H. Abramowicz^{27,u}, I. Abt²¹, L. Adamczyk⁸, M. Adamus³⁴, R. Aggarwal^{4,a}, S. Antonelli², O. Arslan³, V. Aushev^{16,17,o}, Y. Aushev^{17,o,p}, O. Bachynska¹⁰, A.N. Barakbaev¹⁵, N. Bartosik¹⁰, O. Behnke¹⁰, J. Behr¹⁰, U. Behrens¹⁰, A. Bertolin²³, S. Bhadra³⁶, I. Bloch¹¹, V. Bokhonov^{16,o}, E.G. Boos¹⁵, K. Borras¹⁰, I. Brock³, R. Brugnera²⁴, A. Bruni¹, B. Brzozowska³³, P.J. Bussey¹², A. Caldwell²¹, M. Capua⁵, C.D. Catterall³⁶, J. Chwastowski^{7,d}, J. Ciborowski^{33,x}, R. Ciesielski^{10,f}, A.M. Cooper-Sarkar²², M. Corradi¹, F. Corriveau¹⁸, G. D'Agostini²⁶, R.K. Dementiev²⁰, R.C.E. Devenish²², G. Dolinska¹⁰, V. Drugakov¹¹, S. Dusini²³, J. Ferrando¹², J. Figiel⁷, B. Foster^{13,l}, G. Gach⁸, A. Garfagnini²⁴, A. Geiser¹⁰, A. Gizhko¹⁰, L.K. Gladilin²⁰, O. Gogota¹⁷, Yu.A. Golubkov²⁰, J. Grebenyuk¹⁰, I. Gregor¹⁰, G. Grzelak³³, O. Gueta²⁷, M. Guzik⁸, W. Hain¹⁰, G. Hartner³⁶, D. Hochman³⁵, R. Hori¹⁴, Z.A. Ibrahim⁶, Y. Iga²⁵, M. Ishitsuka²⁸, A. Iudin^{17,p}, F. Januschek¹⁰, I. Kadenko¹⁷, S. Kananov²⁷, T. Kanno²⁸, U. Karshon³⁵, M. Kaur⁴, P. Kaur^{4,a}, L.A. Khein²⁰, D. Kisielewska⁸, R. Klanner¹³, U. Klein^{10,g}, N. Kondrashova^{17,q}, O. Kononenko¹⁷, Ie. Korol¹⁰, I.A. Korzhavina²⁰, A. Kotański⁹, U. Kötz¹⁰, N. Kovalchuk^{17,r}, H. Kowalski¹⁰, O. Kuprash¹⁰, M. Kuze²⁸, B.B. Levchenko²⁰, A. Levy²⁷, V. Libov¹⁰, S. Limentani²⁴, M. Lisovyi¹⁰, E. Lobodzinska¹⁰, W. Lohmann¹¹, B. Löhr¹⁰, E. Lohrmann¹³, A. Longhin^{23,t}, D. Lontkovskiy¹⁰, O.Yu. Lukina²⁰, J. Maeda^{28,v}, I. Makarenko¹⁰, J. Malka¹⁰, J.F. Martin³¹, S. Mergelmeyer³, F. Mohamad Idris^{6,c}, K. Mujkic^{10,h}, V. Myronenko^{10,i}, K. Nagano¹⁴, A. Nigro²⁶, T. Nobe²⁸, D. Notz¹⁰, R.J. Nowak³³, K. Olkiewicz⁷, Yu. Onishchuk¹⁷, E. Paul³, W. Perlański^{33,y}, H. Perrey¹⁰, N.S. Pokrovskiy¹⁵, A.S. Proskuryakov²⁰, M. Przybycień⁸, A. Raval¹⁰, P. Roloff^{10,j}, I. Rubinsky¹⁰, M. Ruspa³⁰, V. Samojlov¹⁵, D.H. Saxon¹², M. Schioppa⁵, W.B. Schmidke^{21,s}, U. Schneekloth¹⁰, T. Schörner-Sadenius¹⁰, J. Schwartz¹⁸, L.M. Shcheglova²⁰, R. Shevchenko^{17,p}, O. Shkola^{17,r}, I. Singh^{4,b}, I.O. Skillicorn¹², W. Słomiński^{9,e}, V. Sola¹³, A. Solano²⁹, A. Spiridonov^{10,k}, L. Stanco²³, N. Stefaniuk¹⁰, A. Stern²⁷, T.P. Stewart³¹, P. Stopa⁷, J. Sztuk-Dambietz¹³, D. Szuba¹³, J. Szuba¹⁰, E. Tassi⁵, T. Temiraliev¹⁵, K. Tokushuku^{14,m}, J. Tomaszewska^{33,z}, A. Trofymov^{17,r}, V. Trusov¹⁷, T. Tsurugai¹⁹, M. Turcato¹³, O. Turkot^{10,i}, T. Tymieniecka³⁴, A. Verbitskyi²¹, O. Viazlo¹⁷, R. Walczak²², W.A.T. Wan Abdullah⁶, K. Wichmann^{10,i}, M. Wing^{32,w}, G. Wolf¹⁰, S. Yamada¹⁴, Y. Yamazaki^{14,n}, N. Zakharchuk^{17,r}, A.F. Żarnecki³³, L. Zawiejski⁷, O. Zenaiev¹⁰, B.O. Zhautykov¹⁵, N. Zhmak^{16,o}, D.S. Zotkin²⁰

- 1 *INFN Bologna, Bologna, Italy* ^A
- 2 *University and INFN Bologna, Bologna, Italy* ^A
- 3 *Physikalisches Institut der Universität Bonn, Bonn, Germany* ^B
- 4 *Panjab University, Department of Physics, Chandigarh, India*
- 5 *Calabria University, Physics Department and INFN, Cosenza, Italy* ^A
- 6 *National Centre for Particle Physics, Universiti Malaya, 50603 Kuala Lumpur, Malaysia* ^C
- 7 *The Henryk Niewodniczanski Institute of Nuclear Physics, Polish Academy of Sciences, Krakow, Poland* ^D
- 8 *AGH-University of Science and Technology, Faculty of Physics and Applied Computer Science, Krakow, Poland* ^D
- 9 *Department of Physics, Jagellonian University, Cracow, Poland*
- 10 *Deutsches Elektronen-Synchrotron DESY, Hamburg, Germany*
- 11 *Deutsches Elektronen-Synchrotron DESY, Zeuthen, Germany*
- 12 *School of Physics and Astronomy, University of Glasgow, Glasgow, United Kingdom* ^E
- 13 *Hamburg University, Institute of Experimental Physics, Hamburg, Germany* ^F
- 14 *Institute of Particle and Nuclear Studies, KEK, Tsukuba, Japan* ^G
- 15 *Institute of Physics and Technology of Ministry of Education and Science of Kazakhstan, Almaty, Kazakhstan*
- 16 *Institute for Nuclear Research, National Academy of Sciences, Kyiv, Ukraine*
- 17 *Department of Nuclear Physics, National Taras Shevchenko University of Kyiv, Kyiv, Ukraine*
- 18 *Department of Physics, McGill University, Montréal, Québec, Canada H3A 2T8* ^H
- 19 *Meiji Gakuin University, Faculty of General Education, Yokohama, Japan* ^G
- 20 *Lomonosov Moscow State University, Skobeltsyn Institute of Nuclear Physics, Moscow, Russia* ^I
- 21 *Max-Planck-Institut für Physik, München, Germany*
- 22 *Department of Physics, University of Oxford, Oxford, United Kingdom* ^E
- 23 *INFN Padova, Padova, Italy* ^A
- 24 *Dipartimento di Fisica dell'Università and INFN, Padova, Italy* ^A
- 25 *Polytechnic University, Tokyo, Japan* ^G
- 26 *Dipartimento di Fisica, Università 'La Sapienza' and INFN, Rome, Italy* ^A
- 27 *Raymond and Beverly Sackler Faculty of Exact Sciences, School of Physics, Tel Aviv University, Tel Aviv, Israel* ^J
- 28 *Department of Physics, Tokyo Institute of Technology, Tokyo, Japan* ^G
- 29 *Università di Torino and INFN, Torino, Italy* ^A
- 30 *Università del Piemonte Orientale, Novara, and INFN, Torino, Italy* ^A
- 31 *Department of Physics, University of Toronto, Toronto, Ontario, Canada M5S 1A7* ^H
- 32 *Physics and Astronomy Department, University College London, London, United Kingdom* ^E
- 33 *Faculty of Physics, University of Warsaw, Warsaw, Poland*

- ³⁴ *National Centre for Nuclear Research, Warsaw, Poland*
- ³⁵ *Department of Particle Physics and Astrophysics, Weizmann Institute, Rehovot, Israel*
- ³⁶ *Department of Physics, York University, Ontario, Canada M3J 1P3 ^H*

- ^A supported by the Italian National Institute for Nuclear Physics (INFN)
- ^B supported by the German Federal Ministry for Education and Research (BMBF),
under contract No. 05 H09PDF
- ^C supported by HIR grant UM.C/625/1/HIR/149 and UMRG grants RU006-2013,
RP012A-13AFR and RP012B-13AFR from Universiti Malaya, and ERGS grant
ER004-2012A from the Ministry of Education, Malaysia
- ^D supported by the National Science Centre under contract No. DEC-
2012/06/M/ST2/00428
- ^E supported by the Science and Technology Facilities Council, UK
- ^F supported by the German Federal Ministry for Education and Research (BMBF),
under contract No. 05h09GUF, and the SFB 676 of the Deutsche Forschungsge-
meinschaft (DFG)
- ^G supported by the Japanese Ministry of Education, Culture, Sports, Science and
Technology (MEXT) and its grants for Scientific Research
- ^H supported by the Natural Sciences and Engineering Research Council of Canada
(NSERC)
- ^I supported by RF Presidential grant N 3920.2012.2 for the Leading Scientific Schools
and by the Russian Ministry of Education and Science through its grant for Scientific
Research on High Energy Physics
- ^J supported by the Israel Science Foundation

- ^a also funded by Max Planck Institute for Physics, Munich, Germany
- ^b also funded by Max Planck Institute for Physics, Munich, Germany, now at Sri Guru Granth Sahib World University, Fatehgarh Sahib
- ^c also at Agensi Nuklear Malaysia, 43000 Kajang, Bangi, Malaysia
- ^d also at Cracow University of Technology, Faculty of Physics, Mathematics and Applied Computer Science, Poland
- ^e partially supported by the Polish National Science Centre projects DEC-2011/01/B/ST2/03643 and DEC-2011/03/B/ST2/00220
- ^f now at Rockefeller University, New York, NY 10065, USA
- ^g now at University of Liverpool, United Kingdom
- ^h also affiliated with University College London, UK
- ⁱ supported by the Alexander von Humboldt Foundation
- ^j now at CERN, Geneva, Switzerland
- ^k also at Institute of Theoretical and Experimental Physics, Moscow, Russia
- ^l Alexander von Humboldt Professor; also at DESY and University of Oxford
- ^m also at University of Tokyo, Japan
- ⁿ now at Kobe University, Japan
- ^o supported by DESY, Germany
- ^p member of National Technical University of Ukraine, Kyiv Polytechnic Institute, Kyiv, Ukraine
- ^q now at DESY ATLAS group
- ^r member of National University of Kyiv - Mohyla Academy, Kyiv, Ukraine
- ^s now at BNL, USA
- ^t now at LNF, Frascati, Italy
- ^u also at Max Planck Institute for Physics, Munich, Germany, External Scientific Member
- ^v now at Tokyo Metropolitan University, Japan
- ^w also supported by DESY
- ^x also at Łódź University, Poland
- ^y member of Łódź University, Poland
- ^z now at Polish Air Force Academy in Deblin

1 Introduction

Events containing an isolated high-energy photon can provide a direct probe of the underlying partonic process in high-energy collisions involving hadrons, since the emission of such photons is largely unaffected by parton hadronisation. Processes of this kind have been studied in a number of fixed-target and hadron-collider experiments [1]. In ep collisions at HERA, the ZEUS and H1 collaborations have previously reported the production of isolated photons in photoproduction [2–7], in which the exchanged virtual photon is quasi-real, and also in deep inelastic scattering (DIS) [8–11]. In this paper, earlier photoproduction measurements by ZEUS are extended by using the full HERA II data set. The statistical precision is much improved owing to the availability of higher integrated luminosity. Measurements are presented of isolated-photon production at high transverse energy with and without an explicit accompanying-jet requirement. The measurement of the jet gives further information on the event dynamics.

Figure 1 gives examples of the lowest-order (LO) diagrams for high-energy photoproduction of photons in quantum chromodynamics (QCD). In “direct” production processes, the entire incoming photon is absorbed by a quark from the incoming proton, while in “resolved” processes, the photon’s hadronic structure provides a quark or gluon that interacts with a parton from the proton. Photons that are radiated in the hard scattering process, rather than resulting from meson decay, are commonly called “prompt”¹. Higher-order processes include “fragmentation processes” in which a photon is radiated within a jet, also illustrated in Fig. 1. Such processes are suppressed by requiring that the photon be isolated. Photons radiated at large angles from the incoming or outgoing electron give rise to an observed scattered electron in the detector; such events are excluded from this measurement.

Perturbative QCD predictions are compared to the measurements. The cross sections for isolated-photon production in photoproduction have been calculated to next-to-leading order (NLO) by Fontannaz, Guillet and Heinrich (FGH) [12,13]. Calculations based on the k_T -factorisation approach have been made by Lipatov, Malyshev and Zotov (LMZ) [14–16].

2 Experimental set-up

The measurements are based on a data sample corresponding to an integrated luminosity of $374 \pm 7 \text{ pb}^{-1}$, taken during the years 2004 to 2007 with the ZEUS detector at HERA.

¹ An alternative commonly-used nomenclature is to refer to “prompt” photons as “direct”; thus Figs. 1(a) and 1(b) would be called “direct-direct” and “resolved-direct” diagrams, respectively.

During this period, HERA ran with an electron or positron beam energy of 27.5 GeV and a proton beam energy of 920 GeV. The sample is a sum of e^+p and e^-p data².

A detailed description of the ZEUS detector can be found elsewhere [17]. Charged particles were measured in the central tracking detector (CTD) [18] and a silicon micro vertex detector (MVD) [19] which operated in a magnetic field of 1.43 T provided by a thin superconducting solenoid. The high-resolution uranium-scintillator calorimeter (CAL) [20] consisted of three parts: the forward (FCAL), the barrel (BCAL) and the rear (RCAL) calorimeters. The BCAL covered the pseudorapidity range -0.74 to 1.01 as seen from the nominal interaction point, and the FCAL and RCAL extended the coverage to the range -3.5 to 4.0 . Each part of the CAL was subdivided into elements referred to as cells. The barrel electromagnetic calorimeter (BEMC) cells had a pointing geometry aimed at the nominal interaction point, with a cross section approximately $5 \times 20 \text{ cm}^2$, with the finer granularity in the Z direction³ and the coarser in the (X, Y) plane. This fine granularity allows the use of shower-shape distributions to distinguish isolated photons from the products of neutral meson decays such as $\pi^0 \rightarrow \gamma\gamma$. The CAL energy resolution, as measured under test-beam conditions, was $\sigma(E)/E = 0.18/\sqrt{E}$ for electrons and $0.35/\sqrt{E}$ for hadrons, where E is in GeV.

The luminosity was measured [21] using the Bethe–Heitler reaction $ep \rightarrow e\gamma p$ by a luminosity detector which consisted of two independent systems: a lead-scintillator calorimeter [22] and a magnetic spectrometer [23].

3 Theory

The LO QCD processes relevant to the present measurements are the direct and resolved photoproduction processes (Fig. 1). Higher-order processes include NLO diagrams and fragmentation processes; a box-diagram term also contributes significantly at next-to-next-to-leading order.

Two theoretical predictions are compared to the measurements presented here. In the approach of FGH [12, 13], the LO and NLO diagrams and the box-diagram term are calculated explicitly. Fragmentation processes are also calculated in terms of a fragmentation function in which a quark or gluon gives rise to a photon; an experimentally determined non-perturbative parameterisation is used as input to the theoretical calculation [24].

² Hereafter “electron” refers to both electrons and positrons unless otherwise stated.

³ The ZEUS coordinate system is a right-handed Cartesian system, with the Z axis pointing in the nominal proton beam direction, referred to as the “forward direction”, and the X axis pointing towards the centre of HERA. The coordinate origin is at the centre of the CTD. The pseudorapidity is defined as $\eta = -\ln(\tan \frac{\theta}{2})$, where the polar angle, θ , is measured with respect to the Z axis.

The CTEQ6 [25] and AFG04 [26] parton densities are used for the proton and photon respectively; the use of alternatives altered the results by typically 5%, which was small compared to the other uncertainties on the theory. The authors stress that their NLO calculation must include fragmentation terms to give a well-defined result. Fragmentation and box terms contribute each about 10% to the total cross section. Theoretical uncertainties arise due to the choice of renormalisation, factorisation and fragmentation scales. They were estimated, using a more conservative approach [27] than in the original published paper [12], by varying the renormalisation scale by factors of 0.5 and 2.0, since this gave the largest effect on the cross sections.

The k_T -factorisation method used by LMZ [14–16] makes use of unintegrated parton densities in the proton, using the KMR formalism [28] based on the MRST08 proton parton densities [29]. Fragmentation terms are not included. The box diagram is included together with $2 \rightarrow 3$ subprocesses to represent the LO direct and resolved photon contributions. Uncertainties were evaluated as provided by LMZ.

All results are presented at the hadron level, and to make use of the predictions, cuts equivalent to the experimental kinematic selections including the photon isolation (see Section 5) were applied at the parton level. Hadronisation corrections were then evaluated (Section 4) and applied to each of the calculations to enable the predictions to be compared to the experimental data.

4 Monte Carlo event simulation

Monte Carlo (MC) event samples were generated to evaluate the detector acceptance and event-reconstruction efficiency, and to provide signal and background distributions. The program PYTHIA 6.416 [30] was used to generate the direct and resolved prompt-photon processes, and also $2 \rightarrow 2$ parton-parton scattering processes not involving photons (“dijet events”). For these purposes, CTEQ4 [31] and GRV [32] parton densities were used. The dijet event samples were generated to enable background events to be extracted and used in the analysis. Backgrounds to the isolated photons measured here arise from decays of neutral mesons in hadronic jets where the decay products create an energy cluster in the BCAL that passes the selection criteria for a photon. In PYTHIA dijet events, a photon can also be radiated from an incoming or outgoing quark. Events in which a high-energy photon was radiated from a quark or lepton (“radiative events”) were not included in the final background samples but were defined, in accordance with theory, as a component of the signal.

As a check and to enable systematic uncertainties to be estimated, event samples were also generated using the HERWIG 6.510 program [33]. The cluster-based hadronisation

scheme of HERWIG provides an alternative to the string-based scheme of PYTHIA.

The generated MC events were passed through the ZEUS detector and trigger simulation programs based on GEANT 3.21 [34]. They were then reconstructed and analysed using the same programs as used for the data. The hadronisation corrections to the theory calculations were evaluated using PYTHIA and HERWIG, and lowered the theoretical prediction by typically 10%. PYTHIA and HERWIG are in agreement to a few percent; PYTHIA was used to provide the numbers for the present analysis. No uncertainties were applied to these corrections. They were calculated by running the same jet algorithm and event selections, including the isolation criterion, on the generated partons and on the hadronised final state in the direct and resolved prompt-photon MC events.

5 Event selection and reconstruction

A three-level trigger system was used to select events online [17, 35, 36]. The first-level trigger required a loosely measured track in the CTD and a minimum of energy deposited in the CAL. The event conditions were tightened at the second level, and a high-energy photon candidate was required at the third level. Events were initially selected offline by requiring a high-energy photon candidate of transverse energy > 3.5 GeV recorded in the BCAL. To reduce background from non- ep collisions, events were required to have a reconstructed vertex position, Z_{vtx} , within the range $|Z_{\text{vtx}}| < 40$ cm. No scattered beam electron was permitted in the detector, and photoproduction events were selected by the requirement $0.2 < y_{\text{JB}} < 0.7$, where $y_{\text{JB}} = \sum_i E_i(1 - \cos \theta_i)/2E_e$ and E_e is the energy of the electron beam. Here, E_i is the energy of the i -th CAL cell, θ_i is its polar angle and the sum runs over all cells [37].

Energy-flow objects (EFOs) [38] were constructed from clusters of calorimeter cells with signals, associated with tracks when appropriate. Tracks not associated with calorimeter clusters were also included. Photon candidates were identified as EFOs with no associated track, and with at least 90% of the reconstructed energy measured in the BEMC. Those EFOs with wider electromagnetic showers than are typical for a single photon were accepted to make possible the evaluation of backgrounds. Each event was required to contain a photon candidate with a reconstructed transverse energy, E_T^γ , in the range $6 < E_T^\gamma < 15$ GeV and with pseudorapidity, η^γ , in the range $-0.7 < \eta^\gamma < 0.9$.

Jet reconstruction was performed, making use of all the EFOs in the event including photon candidates, by means of the k_T clustering algorithm [39] in the E -scheme in the longitudinally invariant inclusive mode [40] with the radius parameter set to 1.0. The jets were required to have transverse energy, E_T^{jet} , between 4 and 35 GeV and to lie within the pseudorapidity, η^{jet} , range $-1.5 < \eta^{\text{jet}} < 1.8$. By construction, one of the jets found by this

procedure corresponds to or includes the photon candidate. An additional accompanying jet was required in the non-inclusive measurements; if more than one was found, that with the highest E_T^{jet} was used. In this kinematic region, the resolution of the jet transverse energy was about 15–20%, estimated using MC simulations.

To reduce the fragmentation contribution and the background from the decay of neutral mesons within jets, the photon candidate was required to be isolated from the reconstructed tracks and other hadronic activity. High- E_T photons radiated from beam leptons were also suppressed by requiring no observed scattered lepton in the apparatus. The isolation from tracks was applied to exclude radiating electrons, and was achieved by demanding $\Delta R > 0.2$, where $\Delta R = \sqrt{(\Delta\phi)^2 + (\Delta\eta)^2}$ is the distance to the nearest reconstructed track with momentum greater than 250 MeV in the $\eta - \phi$ plane, where ϕ is the azimuthal angle. This condition was applied only at the detector level, and not in the hadron- or parton-level calculations. Isolation from other hadronic activity was imposed by requiring that the photon-candidate EFO had at least 90% of the total energy of the reconstructed jet of which it formed a part. These selections gave 17441 events with an inclusive-photon candidate and 12450 events with a photon candidate and an accompanying jet.

6 Extraction of the photon signal

The selected samples contain a large admixture of background events in which one or more neutral mesons, such as π^0 and η , decayed to photons, thereby producing a photon candidate in the BEMC. The photon signal was extracted statistically following the approach used in previous ZEUS analyses [8–11].

The photon signal was extracted from the background using the energy-weighted width, measured in the Z direction, of the BEMC energy-cluster comprising the photon candidate. This width was calculated as $\langle\delta Z\rangle = \sum_i E_i |Z_i - Z_{\text{cluster}}| / (w_{\text{cell}} \sum_i E_i)$. Here, Z_i is the Z position of the centre of the i -th cell, Z_{cluster} is the energy-weighted centroid of the EFO cluster, w_{cell} is the width of the cell in the Z direction, and E_i is the energy recorded in the cell. The sum runs over all BEMC cells in the EFO.

The global distribution of $\langle\delta Z\rangle$ in the data and in the PYTHIA MC are shown in Fig. 2 for inclusive photon events and those containing an additional jet. The $\langle\delta Z\rangle$ distribution exhibits a double-peaked structure with the first peak at ≈ 0.1 , associated with the photon signal, and the second peak at ≈ 0.5 , dominated by the $\pi^0 \rightarrow \gamma\gamma$ component of the background.

The number of isolated-photon events in the data is determined by a χ^2 fit to the $\langle\delta Z\rangle$

distribution in the range $0.05 < \langle \delta Z \rangle < 0.8$, varying the relative fractions of the signal and background components as represented by histogram templates obtained from the MC. This is illustrated in Fig. 2, and a corresponding fit was performed for each measured cross section bin, with χ^2 values of typically 1.1 per degree of freedom (i.e. 31/28). The extracted signals corresponded overall to 8193 ± 156 inclusive-photon events and 6262 ± 132 events with a photon and an accompanying jet.

A bin-by-bin correction method was used to determine the production cross section, by means of the relationship

$$\frac{d\sigma}{dY} = \frac{\mathcal{A} N(\gamma)}{\mathcal{L} \Delta Y}, \quad (1)$$

where $N(\gamma)$ is the number of photons in a bin as extracted from the fit, in events accompanied by a jet if required, and ΔY is the bin width, \mathcal{L} is the total integrated luminosity, and \mathcal{A} is the acceptance correction. The acceptance correction was calculated, using MC samples, as the ratio of the number of events that were generated in the given bin to the number that were obtained in the bin after event reconstruction. Its value was typically 1.2. To evaluate the acceptances, allowance must be made for the different acceptances for the direct and the resolved processes, as modelled by PYTHIA. These components can be substantially distinguished by means of events containing a photon and a jet, in which the quantity

$$x_{\gamma}^{\text{meas}} = \frac{E^{\gamma} + E^{\text{jet}} - p_Z^{\gamma} - p_Z^{\text{jet}}}{E^{\text{all}} - p_Z^{\text{all}}}. \quad (2)$$

is a measure of the fraction of the incoming photon energy given to the final-state photon and jet, at a lowest-order approximation. The energies and longitudinal momentum components of the photon (γ), the jet and all of the EFOs in the event were combined as indicated. Figure 3 shows the x_{γ}^{meas} distribution; a peak close to unity is seen, which can be attributed to direct events, and a tail at lower values due to resolved events. A reasonable phenomenological description of the data can be obtained using a MC sample consisting of a 50:40 mixture of PYTHIA-simulated direct and resolved events, as normalised to the data, with a 10% admixture of radiative events divided equally between direct and resolved. The acceptance factors were calculated using this model. Acceptance factors calculated in this way were applied both to the inclusive and to the jet data.

The trigger efficiency was approximately flat above a photon transverse energy of 4.5 GeV, with a value of $87 \pm 2\%$. This includes a correction of 3.6% which was applied to the trigger acceptance modelled by the MC. The correction was evaluated using DIS samples, in data and MC, in which events with prompt photons were triggered in an independent way.

A correction of typically 2% was applied to subtract a contamination of the sample by DIS events, which was determined using MC-simulated DIS samples [11].

7 Systematic uncertainties

The most significant sources of systematic uncertainty were evaluated as follows:

- to allow for uncertainties in the simulation of the hadronic final state, the cross sections were recalculated using HERWIG to model the signal and background events. The ensuing changes in the results correspond to an uncertainty of typically up to 8%, but rising to 18% in the highest bin of x_{γ}^{meas} ;
- the energy of the photon candidate was varied by $\pm 2\%$ in the MC at the detector level. This value was obtained from a study of energy-momentum conservation in Deeply Virtual Compton Scattering events measured in the ZEUS detector, in which the final state consisted of a photon and a scattered electron. Independently, the energy of the accompanying jet, when measured, was varied by an amount decreasing from $\pm 4.5\%$ to $\pm 2.5\%$ as E_T^{jet} increases from 4 GeV to above 10 GeV. These values were obtained as described in a previous ZEUS publication [11]. Each of these contributions gave variations in the measured cross sections of typically 5%.

Further systematic uncertainties were evaluated as follows:

- the uncertainty in the acceptance due to the estimation of the relative fractions of direct and resolved events and radiative events in the MC sample was estimated by varying these fractions by $\pm 15\%$ and $\pm 5\%$ respectively in absolute terms; the changes in the cross sections were typically $\pm 2\%$ in each case;
- the dependence of the result on the modelling of the hadronic background by the MC was investigated by varying the upper limit for the $\langle \delta Z \rangle$ fit in the range $[0.6, 1.0]$; this gave a $\pm 2\%$ variation.

Other sources of systematic uncertainty were found to be negligible and were ignored. These included the modelling of the track-isolation cut, the track-momentum cut, and the cuts on photon isolation, the electromagnetic fraction of the photon shower, y_{JB} and Z_{vtx} . Except for the uncertainty on the modelling of the hadronic final state, the major uncertainties were treated as symmetric, and all the uncertainties were combined in quadrature. The common uncertainties of 2.0% on the trigger efficiency and 1.9% on the luminosity measurement were not included in the tables and figures.

8 Results

Differential cross sections were measured for the production of an isolated photon inclusively, and with at least one accompanying jet, in the kinematic region defined by $Q^2 < 1 \text{ GeV}^2$, $0.2 < y < 0.7$, $-0.7 < \eta^\gamma < 0.9$, $6 < E_T^\gamma < 15 \text{ GeV}$, and where relevant $4 < E_T^{\text{jet}} < 35 \text{ GeV}$ and $-1.5 < \eta^{\text{jet}} < 1.8$. All quantities were evaluated at the hadron level in the laboratory frame. Again, the jets were formed according to the k_T clustering algorithm with the radius parameter set to 1.0. Photon isolation was imposed such that at least 90% of the energy of the jet-like object containing the photon originated from the photon. If more than one accompanying jet was found within the designated η^{jet} range in an event, that with highest E_T^{jet} was taken. The integrated luminosity was $374 \pm 7 \text{ pb}^{-1}$.

The differential cross sections as functions of E_T^γ , η^γ , E_T^{jet} , η^{jet} and x_γ^{meas} are shown in Figs. 4–6, and 7, and given in Tables 1–7. Cross sections in E_T^{jet} above 15 GeV are omitted from Table 5 and Fig. 6(a) owing to limited statistics, but this kinematic region is included in the other cross-section measurements. The theoretical predictions described in Section 3 are compared to the measurements; theoretical uncertainties are indicated by the width of the respective shaded areas. The NLO-based predictions from FGH describe the distributions well. The predictions of LMZ, within their uncertainties, also describe the photon distributions well, but give a less good description at low η^{jet} and low x_γ^{meas} . The experimental uncertainties are substantially smaller than those of the theory.

9 Conclusions

The production of inclusive isolated photons and photons with an accompanying jet has been measured in photoproduction with the ZEUS detector at HERA using an integrated luminosity of $374 \pm 7 \text{ pb}^{-1}$. The present results improve on earlier ZEUS results, which were made with lower integrated luminosities. Differential cross sections are presented as functions of the transverse energy and the pseudorapidity of the photon and the jet, and x_γ^{meas} , where the kinematic region is defined in the laboratory frame by: $Q^2 < 1 \text{ GeV}^2$, $0.2 < y < 0.7$, $-0.7 < \eta^\gamma < 0.9$, $6 < E_T^\gamma < 15 \text{ GeV}$ and, where a jet is required, $4 < E_T^{\text{jet}} < 35 \text{ GeV}$ and $-1.5 < \eta^{\text{jet}} < 1.8$. Photon isolation was imposed such that at least 90% of the energy of the jet-like object containing the photon originated from the photon. The NLO-based predictions of Fontannaz, Guillet and Heinrich reproduce the measured experimental distributions well. The k_T -factorisation approach of Lipatov, Malyshev and Zotov describes the photon distributions well but gives a less good description of the jet-based variables.

Acknowledgements

We appreciate the contributions to the construction, maintenance and operation of the ZEUS detector made by many people who are not listed as authors. The HERA machine group and the DESY computing staff are especially acknowledged for their success in providing excellent operation of the collider and the data-analysis environment. We thank the DESY directorate for their strong support and encouragement. We also thank M. Fontannaz, G. Heinrich, A. Lipatov, M. Malyshev and N. Zotov for providing assistance and theoretical results.

References

- [1] P. Aurenche et al., Phys. Rev. D 73 (2006) 094007;
CDF Collaboration, T. Aaltonen et al., Phys. Rev. Lett. 95 (2005) 022003;
DØ Collaboration, V.M. Abazov et al., Phys. Lett. B 639 (2006) 151;
DØ Collaboration, V.M. Abazov et al., arXiv 1308.2708 (2013);
ATLAS Collaboration, G. Aad et al., Nucl. Phys. B 875 (2013) 483;
ATLAS Collaboration, G. Aad et al., arXiv 1311.1440 (2013) ;
CMS Collaboration, S. Chatrchyan et al., Phys. Rev. D 84 (2011) 052011;
CMS Collaboration, S. Chatrchyan et al., Phys. Lett. B 710 (2012) 403.
- [2] ZEUS Collaboration, J. Breitweg et al., Phys. Lett. B 413 (1997) 201.
- [3] ZEUS Collaboration, J. Breitweg et al., Phys. Lett. B 472 (2000) 175.
- [4] ZEUS Collaboration, S. Chekanov et al., Phys. Lett. B 511 (2001) 19.
- [5] ZEUS Collaboration, S. Chekanov et al., Eur. Phys. J. C 49 (2007) 511.
- [6] H1 Collaboration, A. Aktas et al., Eur. Phys. J. C 38 (2004) 437.
- [7] H1 Collaboration, F.D. Aaron et al., Eur. Phys. J. C 66 (2010) 17.
- [8] H1 Collaboration, F.D. Aaron et al., Eur. Phys. J. C 54 (2008) 371.
- [9] ZEUS Collaboration, S. Chekanov et al., Phys. Lett. B 595 (2004) 86.
- [10] ZEUS Collaboration, S. Chekanov et al., Phys. Lett. B 687 (2010) 16.
- [11] ZEUS Collaboration, H. Abramowicz et al., Phys. Lett. B 715 (2012) 88.
- [12] M. Fontannaz, J.Ph. Guillet and G. Heinrich, Eur. Phys. J. C 21 (2001) 303.
- [13] M. Fontannaz and G. Heinrich, Eur. Phys. J. C 34 (2004) 191.
- [14] A.V. Lipatov and N.P. Zotov, Phys. Rev. D 72 (2005) 054002.
- [15] A.V. Lipatov and N.P. Zotov, Phys. Rev. D 81 (2010) 094027.
- [16] A.V. Lipatov, M.A. Malyshev and N.P. Zotov, Phys. Rev. D 88 (2013) 074001.
- [17] ZEUS Collaboration, U. Holm (ed.), *The ZEUS Detector*. Status Report (unpublished), DESY (1993), available on <http://www-zeus.desy.de/bluebook/bluebook.html>.
- [18] N. Harnew et al., Nucl. Inst. Meth. A 279 (1989) 290;
B. Foster et al., Nucl. Phys. Proc. Suppl. B 32 (1993) 181;
B. Foster et al., Nucl. Inst. Meth. A 338 (1994) 254.
- [19] A. Polini et al., Nucl. Inst. Meth. A 581 (2007) 656.

- [20] M. Derrick et al., Nucl. Inst. Meth. A 309 (1991) 77;
A. Andresen et al., Nucl. Inst. Meth. A 309 (1991) 101;
A. Caldwell et al., Nucl. Inst. Meth. A 321 (1992) 356;
A. Bernstein et al., Nucl. Inst. Meth. A 336 (1993) 23.
- [21] L. Adamczyk et al., arXiv:1306.1391 (2013).
- [22] J. Andruszków et al., Preprint DESY-92-066, DESY, 1992;
ZEUS Collaboration, M. Derrick et al., Z. Phys. C 63 (1994) 391;
J. Andruszków et al., Acta Phys. Pol. B 32 (2001) 2025.
- [23] M. Heilbich et al., Nucl. Inst. Meth. A 565 (2006) 572.
- [24] L. Bourhis et al., Eur. Phys. J. C 19 (2001) 89.
- [25] J. Pumplin et al., JHEP 02 (2006) 032 .
- [26] P. Aurenche, M. Fontannaz and J-P. Guillet, Eur. Phys. J. C 44 (2005) 395.
- [27] M. Fontannaz and G. Heinrich, private communication (2013).
- [28] M. A. Kimber, A. D. Martin and M. G. Ryskin, Phys. Rev. D 63 (2001) 114027;
G. Watt, A. D. Martin and M. G. Ryskin, Eur. Phys. J. C 31 (2003) 73.
- [29] A. D. Martin, J. Stirling, R. Thorne and G. Watt, Eur. Phys. J. C 63 (2009) 189.
- [30] T. Sjöstrand et al., JHEP 05 (2006) 26.
- [31] H. L. Lai et al., Phys. Rev. D 55 (1997) 1280.
- [32] M. Glück, G. Reya and A. Vogt, Phys. Rev. D 45 (1992) 3986;
Phys. Rev. D 46 (1992) 1973.
- [33] G. Corcella et al., JHEP 0101 (2001) 010.
- [34] R. Brun et al., GEANT3, Technical Report CERN-DD/EE/84-1, CERN, 1987.
- [35] W.H. Smith, K. Tokushuku and L.W. Wiggers, *Proc. Computing in High-Energy Physics (CHEP), Annecy, France, Sept. 1992*, C. Verkerk and W. Wojcik (eds.), p. 222. CERN, Geneva, Switzerland (1992). Also in preprint DESY 92-150B.
- [36] P. Allfrey et al., Nucl. Inst. Meth. A 580 (2007) 1257.
- [37] ZEUS Collaboration, M. Derrick et al., Phys. Lett. B 303 (1993) 183.
- [38] ZEUS Collaboration, J. Breitweg et al., Eur. Phys. J. C 1 (1998) 81;
ZEUS Collaboration, J. Breitweg et al., Eur. Phys. J. C 6 (1999) 43.
- [39] S. Catani et al., Nucl. Phys. B 406 (1993) 187.
- [40] S.D. Ellis and D.E. Soper, Phys. Rev. D 48 (1993) 3160.

E_T^γ range (GeV)	$\frac{d\sigma}{dE_T^\gamma}$ (pb GeV $^{-1}$)	had. corr.
6 – 7	9.75 ± 0.39 (stat.) $^{+0.75}_{-0.35}$ (syst.)	0.88
7 – 8.5	5.91 ± 0.22 (stat.) $^{+0.33}_{-0.31}$ (syst.)	0.90
8.5 – 10	3.08 ± 0.16 (stat.) $^{+0.20}_{-0.20}$ (syst.)	0.93
10 – 15	1.06 ± 0.05 (stat.) $^{+0.06}_{-0.09}$ (syst.)	0.96

Table 1: Measured differential cross-section $\frac{d\sigma}{dE_T^\gamma}$ for inclusive photons. The multiplicative hadronisation correction applied to the theory is given under “had. corr.”.

η^γ range	$\frac{d\sigma}{d\eta^\gamma}$ (pb)	had. corr.
−0.7 – −0.3	19.48 ± 0.77 (stat.) $^{+1.91}_{-1.27}$ (syst.)	0.94
−0.3 – 0.1	21.94 ± 0.76 (stat.) $^{+1.12}_{-1.12}$ (syst.)	0.92
0.1 – 0.5	18.24 ± 0.76 (stat.) $^{+0.87}_{-1.07}$ (syst.)	0.89
0.5 – 0.9	10.19 ± 0.75 (stat.) $^{+0.76}_{-0.20}$ (syst.)	0.88

Table 2: Measured differential cross-section $\frac{d\sigma}{d\eta^\gamma}$ for inclusive photons, and hadronisation correction.

E_T^γ range (GeV)	$\frac{d\sigma}{dE_T^\gamma}$ (pb GeV $^{-1}$)	had. corr.
6 – 7	6.88 ± 0.33 (stat.) $^{+0.55}_{-0.41}$ (syst.)	0.83
7 – 8.5	4.60 ± 0.19 (stat.) $^{+0.28}_{-0.25}$ (syst.)	0.87
8.5 – 10	2.55 ± 0.14 (stat.) $^{+0.17}_{-0.19}$ (syst.)	0.90
10 – 15	0.90 ± 0.04 (stat.) $^{+0.05}_{-0.07}$ (syst.)	0.93

Table 3: Measured differential cross-section $\frac{d\sigma}{dE_T^\gamma}$ for photons accompanied by a jet, and hadronisation correction.

η^γ range	$\frac{d\sigma}{d\eta^\gamma}$ (pb)	had. corr.
−0.7 – −0.3	14.80 ± 0.66 (stat.) $^{+1.24}_{-1.14}$ (syst.)	0.90
−0.3 – 0.1	16.86 ± 0.66 (stat.) $^{+0.97}_{-0.97}$ (syst.)	0.88
0.1 – 0.5	14.43 ± 0.67 (stat.) $^{+0.75}_{-0.97}$ (syst.)	0.86
0.5 – 0.9	7.95 ± 0.66 (stat.) $^{+0.67}_{-0.23}$ (syst.)	0.85

Table 4: Measured differential cross-section $\frac{d\sigma}{d\eta^\gamma}$ for photons accompanied by a jet, and hadronisation correction.

E_T^{jet} range (GeV)	$\frac{d\sigma}{dE_T^{\text{jet}}}$ (pb GeV ⁻¹)	had. corr.
4 – 6	2.64 ± 0.13 (stat.) $^{+0.26}_{-0.21}$ (syst.)	0.86
6 – 8	3.31 ± 0.15 (stat.) $^{+0.21}_{-0.19}$ (syst.)	0.79
8 – 10	2.58 ± 0.13 (stat.) $^{+0.22}_{-0.24}$ (syst.)	0.90
10 – 15	0.87 ± 0.05 (stat.) $^{+0.07}_{-0.07}$ (syst.)	0.98

Table 5: Measured differential cross-section $\frac{d\sigma}{dE_T^{\text{jet}}}$ for photons accompanied by a jet, and hadronisation correction.

η^{jet} range	$\frac{d\sigma}{d\eta^{\text{jet}}}$ (pb)	had. corr.
-1.5 – -0.7	2.46 ± 0.22 (stat.) $^{+0.21}_{-0.22}$ (syst.)	0.71
-0.7 – 0.1	7.85 ± 0.36 (stat.) $^{+0.39}_{-0.31}$ (syst.)	0.80
0.1 – 0.9	9.42 ± 0.37 (stat.) $^{+0.47}_{-0.51}$ (syst.)	0.96
0.9 – 1.8	6.71 ± 0.31 (stat.) $^{+0.34}_{-0.43}$ (syst.)	1.11

Table 6: Measured differential cross-section $\frac{d\sigma}{d\eta^{\text{jet}}}$ for photons accompanied by a jet, and hadronisation correction.

x_γ^{meas} range	$\frac{d\sigma}{dx_\gamma^{\text{meas}}}$ (pb)	had. corr.
0.1 – 0.4	4.66 ± 0.54 (stat.) $^{+0.40}_{-0.41}$ (syst.)	0.67
0.4 – 0.6	13.18 ± 1.07 (stat.) $^{+0.95}_{-1.05}$ (syst.)	0.88
0.6 – 0.7	20.77 ± 1.62 (stat.) $^{+1.05}_{-3.06}$ (syst.)	0.98
0.7 – 0.8	28.42 ± 1.83 (stat.) $^{+1.76}_{-3.13}$ (syst.)	1.32
0.8 – 0.9	50.07 ± 2.30 (stat.) $^{+2.92}_{-3.81}$ (syst.)	1.72
0.9 – 1.0	79.23 ± 3.41 (stat.) $^{+14.95}_{-4.62}$ (syst.)	0.68

Table 7: Measured differential cross-section $\frac{d\sigma}{dx_\gamma^{\text{meas}}}$ for photons accompanied by a jet, and hadronisation correction.

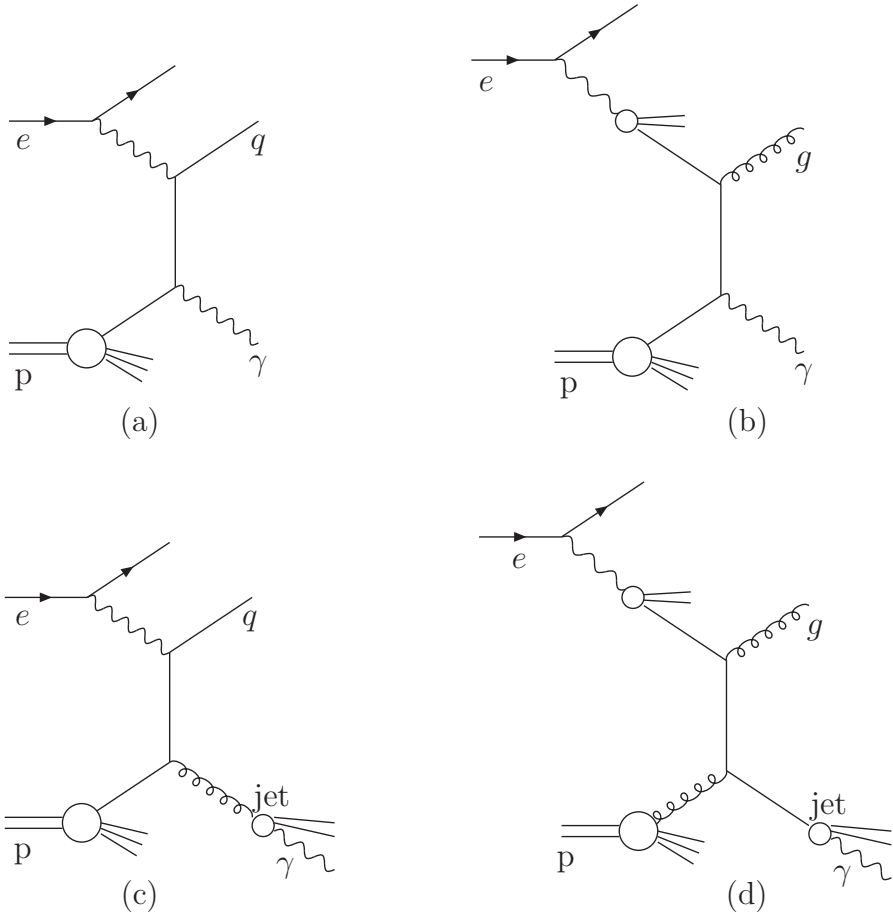
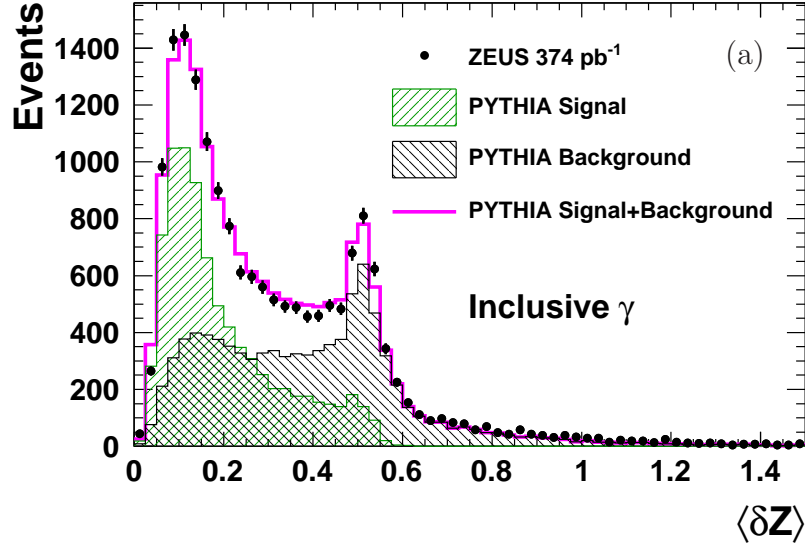


Figure 1: Examples of (a) direct-prompt and (b) resolved-prompt processes at leading order in QCD, and the related (c) direct and (d) resolved fragmentation processes.

ZEUS



ZEUS

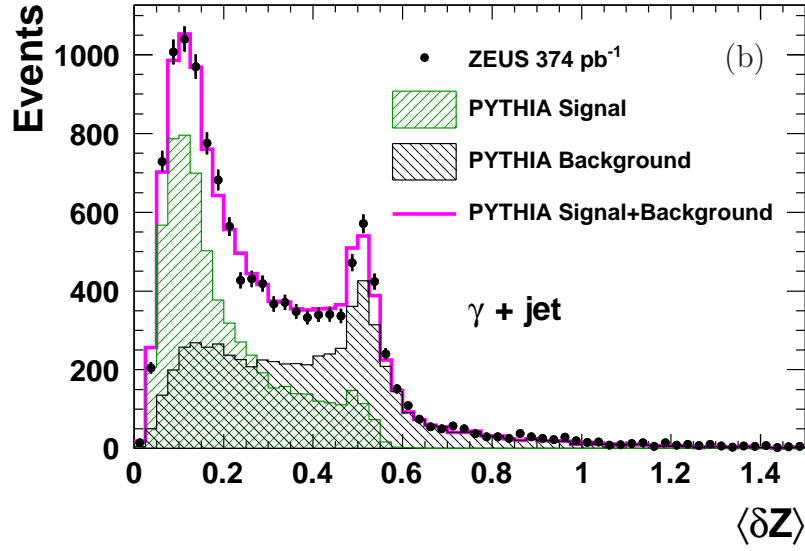


Figure 2: Distributions of $\langle \delta Z \rangle$ for (a) inclusive photon events, (b) events with a photon and an additional jet, showing the fitted signal and background components and their sum. The error bars denote the statistical uncertainties on the data.

ZEUS

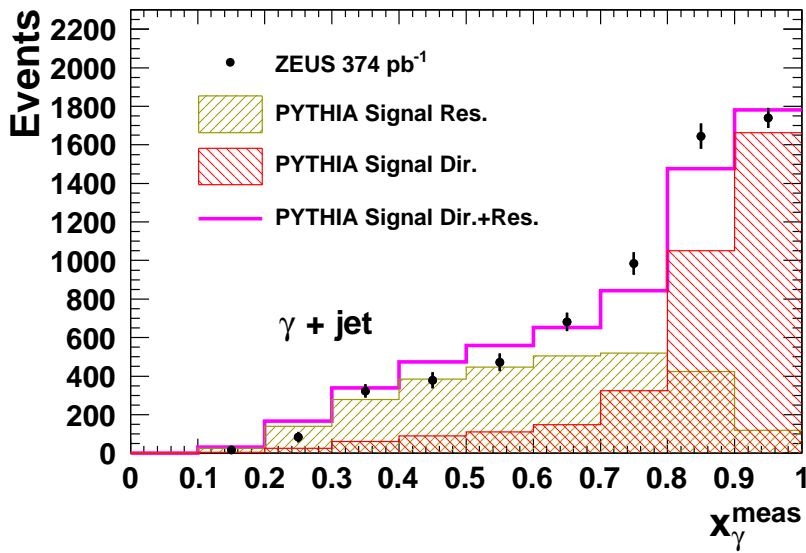
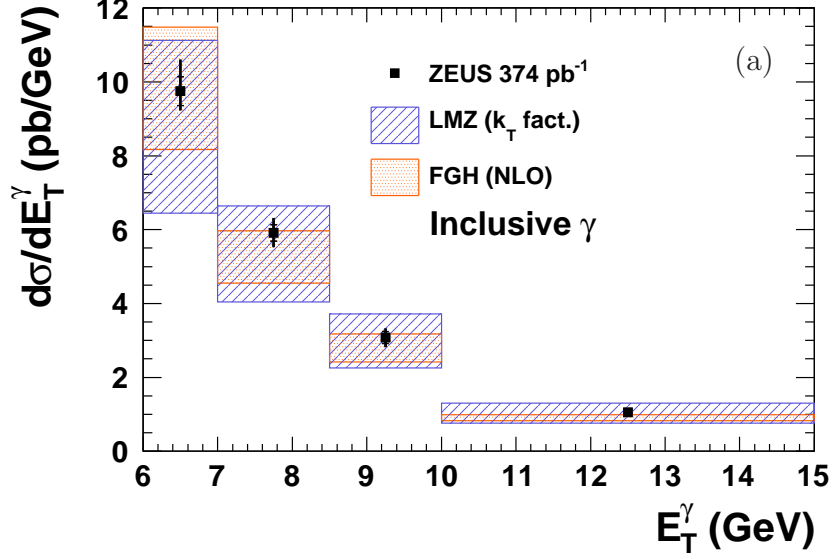


Figure 3: Events detected for different values of x_{γ}^{meas} , compared to a mixture of PYTHIA-generated direct and resolved events, using the model described in the text. The simulated events were passed through the detector simulation. The kinematic ranges of the photons and the jets are described in the text. No acceptance corrections were applied at this stage.

ZEUS



ZEUS

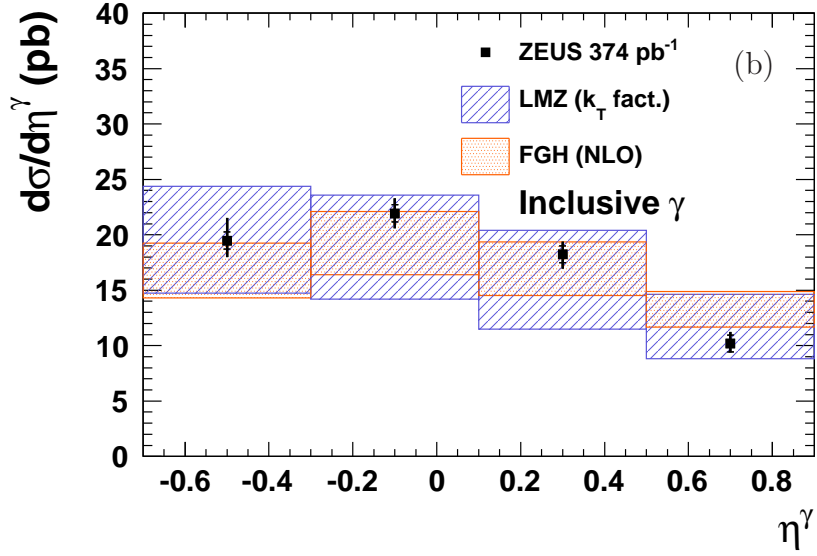
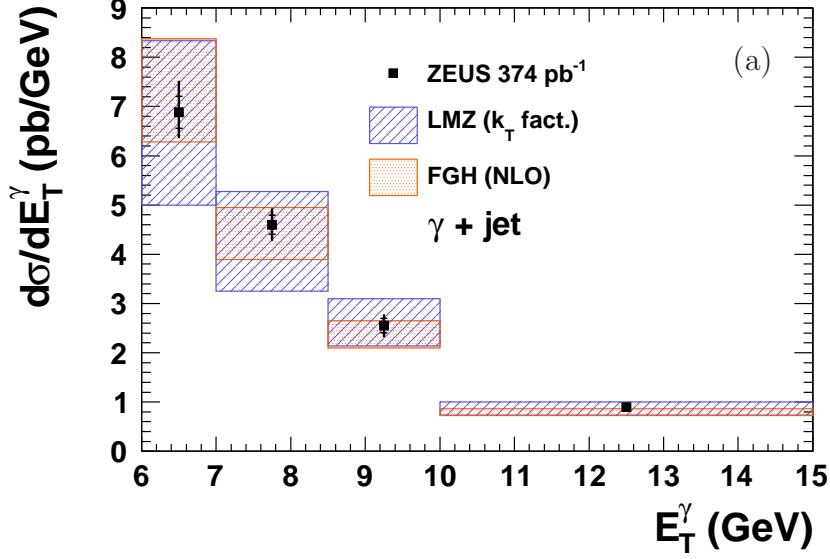


Figure 4: Differential cross sections as functions of (a) E_T^γ and (b) η^γ for events containing an isolated photon, compared to predictions from FGH and LMZ. The kinematic region of the measurement is described in the text. The inner and outer error bars respectively denote statistical uncertainties and statistical uncertainties combined with systematic uncertainties in quadrature. The theoretical uncertainties are shown as hatched and dotted bands.

ZEUS



ZEUS

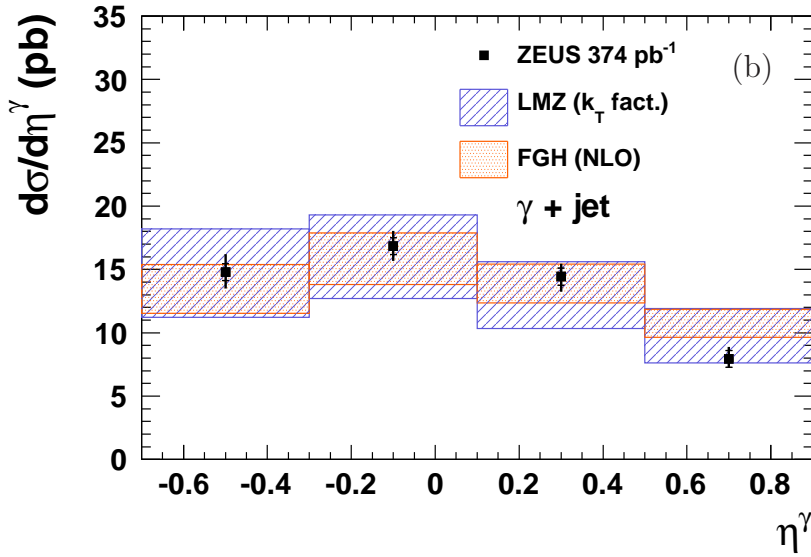
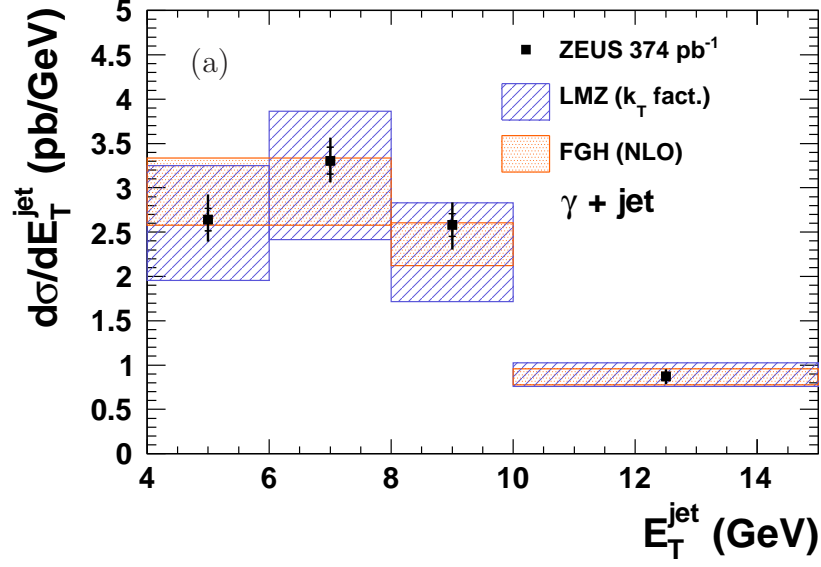


Figure 5: *Differential cross sections as functions of (a) E_T^γ and (b) η^γ , for events containing an isolated photon accompanied by a jet, compared to predictions from FGH and LMZ. The kinematic region of the measurement is described in the text. The inner and outer error bars respectively denote statistical uncertainties and statistical uncertainties combined with systematic uncertainties in quadrature. The theoretical uncertainties are shown as hatched and dotted bands.*

ZEUS



ZEUS

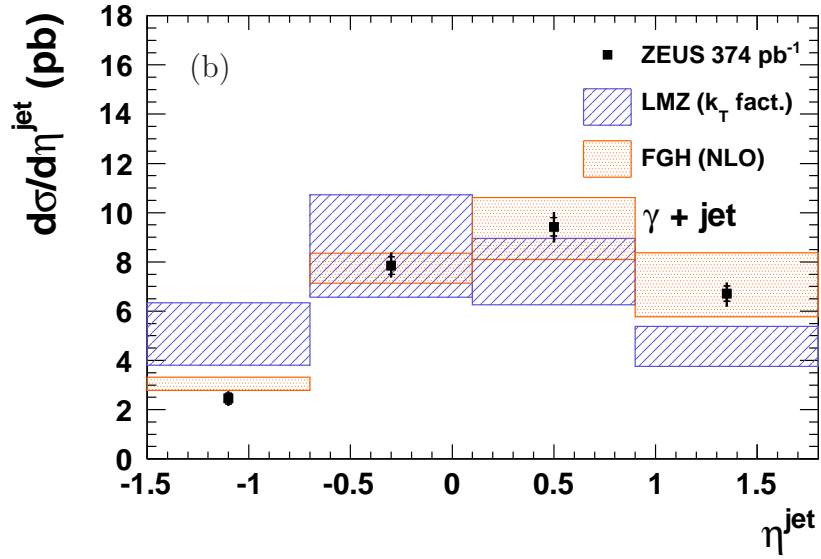


Figure 6: Differential cross sections as functions of (a) E_T^{jet} and (b) η^{jet} , for events containing an isolated photon accompanied by a jet, compared to predictions from FGH and LMZ. The kinematic region of the measurement is described in the text. The inner and outer error bars respectively denote statistical uncertainties and statistical uncertainties combined with systematic uncertainties in quadrature. The theoretical uncertainties are shown as hatched and dotted bands. The first two FGH points in (a) have been averaged into a single bin for calculational reasons.

ZEUS

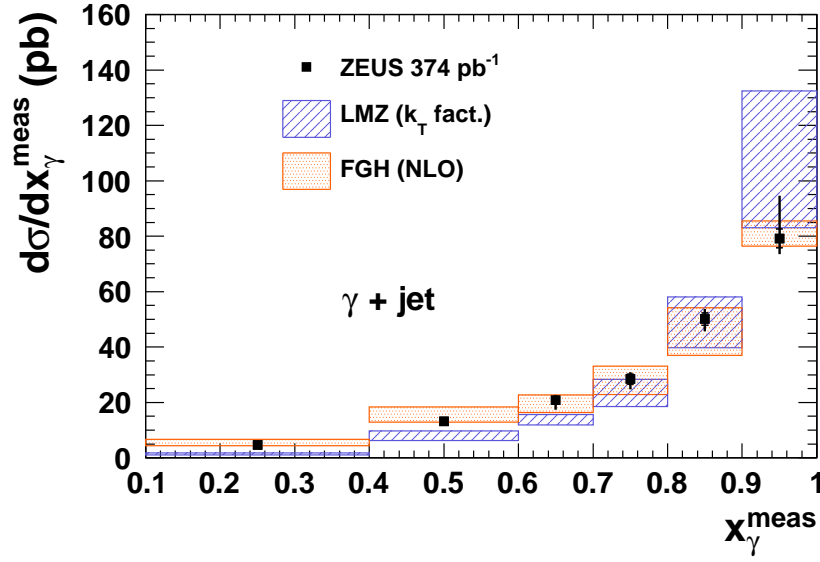


Figure 7: *Differential cross section as a function of x_γ^{meas} , for events containing an isolated photon and a jet, compared to predictions from FGH and LMZ. The kinematic region of the measurement is described in the text. The inner and outer error bars respectively denote statistical uncertainties and statistical uncertainties combined with systematic uncertainties in quadrature. The theoretical uncertainties are shown as hatched and dotted bands.*